Inorganic Chemistry

Article

pubs.acs.org/IC

Structural and Mechanical Properties of Platinum Carbide

Qian Li,[†] Xinxin Zhang,[†,‡] Hanyu Liu,[†] Hui Wang,*[,†] Miao Zhang,[†,§] Quan Li,*[,†] and Yanming Ma[†]

[†]State Key Laboratory of Superhard Materials and College of Materials Science and Engineering, Jilin University, Changchun 130012, China

[‡]Mathematics and Physics Department, Shenyang University of Chemical Technology, Shenyang 110142, China

[§]College of Physics, Beihua University, Jilin 132013, China

ABSTRACT: Platinum carbide (PtC) was synthesized under extreme conditions and considered as a potential candidate for superhard materials. However, the unsettled issue concerning the structural identification has impeded the full understanding of its physical and chemical properties. Here, we examine by first-principles calculations the crystal structure under high pressure and ideal strength along several high-symmetry directions under large deformation. The current calculations reveal that the zinc blende structure is the thermodynamically stable phase, and the simulated X-ray diffraction data are in excellent agreement with the experimental pattern. Further strain−stress calculations indicate that anomalous fluctuating behaviors of ideal strength occur in PtC. These results are expected to broaden our understanding of the structural and mechanical properties for other potential superhard materials formed by heavy transition metals and light elements.

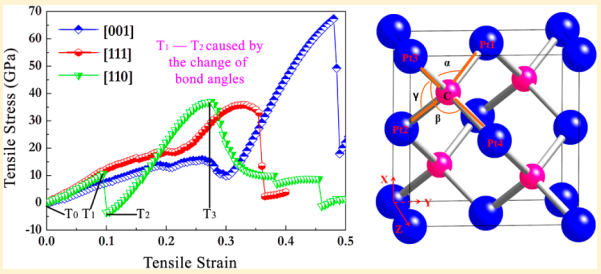

INTRODUCTION

Over the past decades, extensive experimental and theoretical efforts have been devoted to searching new superhard materials that are of great importance in science and technology.[1−3] In general, two groups of materials are commonly considered as potential candidates for superhard materials: (i) the strong covalent compounds formed by light elements, e.g., boron, carbon, nitrogen, and oxygen,[4−7] and (ii) the partially covalent heavy transition-metal borides, carbides, and nitrides, since heavy transition metals can basically introduce high valence electron density into the compounds to resist both elastic and plastic deformation.[8−15] Among them, heavy transition-metal carbides are rarely reported due to the experimental difficulty in synthesis. Encouragingly, Ono et al. successfully synthesized PtC with a high bulk modulus of 301 (±15) GPa by a laser-heated technique under high-temperature and high-pressure conditions.[16] The synthesis of PtC has motivated extensive theoretical efforts to explore its physical and chemical properties.

The knowledge of crystallography is of fundamental importance to condensed matter physics because the physical and chemical properties of materials are determined by the crystal structures. Because of the small scattering cross section of carbon atoms and their ability to form sp-, sp^2-, and sp^3-hybridized bonds, it remains a major challenge to determine the crystal structure of PtC. Through the analysis of X-ray diffraction (XRD) data, Ono et al. proposed that the synthesized PtC crystallizes in a rock-salt (RS) structure.[16] Using a substitution method, several structures were theoretically proposed as ambient- and high-pressure phases of the synthesized PtC, e.g., cubic zinc blende (ZB), nickel−arsenide, and PbO structures.[17−28] Thus, the crystal structure of PtC is the subject of continuing debate. The conflictions encourage us to explore the crystal structure and the mechanical properties of PtC.

Here, we examine the crystal structure for PtC using specially designed calculations under high-pressure conditions. The synthesized PtC adopts the ZB structure at 0−7.2 GPa, and the invariable platinum sublattice in PtC is responsible for the nearly identical XRD under high pressure. The ideal strength calculations show that anomalous fluctuating behaviors of ideal strength occur in ZB PtC induced by intriguing changes of bond angles in the stretching and shearing process.

COMPUTATIONAL DETAILS

We carried out first-principles energetic calculations using the density functional theory within the local density approximation (LDA),[29,30] as implemented in the Vienna Ab initio Simulation Package (VASP).[31] The projector-augment wave method[32] was adopted with a plane-wave kinetic-energy cutoff of 520 eV to give excellent convergence on the total energies and structural parameters. The appropriate Monkhorst−Pack (MP) k meshes[33] of 0.025 $Å^{-1}$ were chosen to ensure that all the structures are well-converged to better than 1 meV per formula. The phonon frequencies were calculated using the direct supercell method.[31] This method uses the forces obtained by the Hellmann−Feynman theorem calculated from the optimized supercell. Convergence check gave the use of 4 × 4 × 4 supercells (128 atoms). Accurate crystal elastic constants were determined from evaluation of stress tensor generated small strain, and the bulk modulus, shear modulus, Young's modulus, and Poisson's ratio were thus estimated by using the Voigt−Reuss−Hill approximation.[34] The microhardness model based on bond strength with the consideration of the roles of metallic components and d valence electrons[35] was used for the

Received: March 20, 2014
Published: May 15, 2014

   dx.doi.org/10.1021/ic5006133 | Inorg. Chem. 2014, 53, 5797−5802

hardness calculation with all the input parameters obtained from first-principles calculations. The ideal strength and relaxed loading path in various directions were determined using a method described previously.[7,36−38]

RESULTS AND DISCUSSION

First, we have ruled out the earlier proposed nickel−arsenide and PbO structures by evidence of the mismatching XRD patterns with experimental data. As shown in Figure 1, if all the

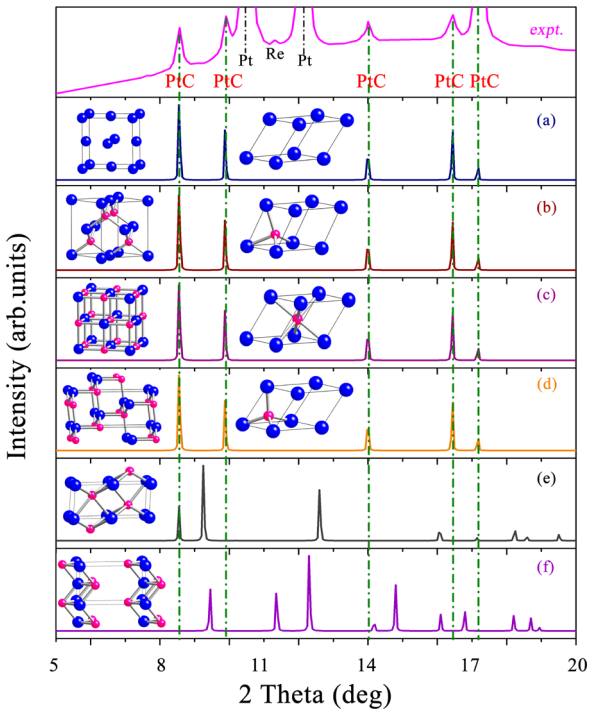

Figure 1. Simulated X-ray diffraction pattern of (a) fcc platinum lattice, (b) ZB phase PtC, (c) RS phase PtC, (d) PtC-0.3, (e) nickel−arsenide phase, and (f) PbO structure. The experimental data from ref 16 is also shown for comparison. The X-ray beam with a wavelength of λ = 0.42 Å (experimental value)[16] was used.

platinum atoms are forced to occupy the face-centered cubic (fcc) sublattice site with the lattice constants equal to 4.814 Å (experimental value), the simulated XRD patterns always fit well with the experimental XRD data at zero pressure wherever carbon atoms occupy. The fact is associated with the small cross section of the C atom and the large Pt/C atomic mass ratio. Therefore, it is impossible to determine carbon atom positions in PtC only through the experimental XRD data. It is noteworthy that platinum atoms have the same occupied atomic positions in both ZB and RS structures, explaining why two previous structures reproduce the experimental XRD pattern.[17−24]

It is of fundamental importance to check the phonon spectra of the ZB and RS structures, since they provide crucial information on structural stabilities. As shown in Figure 2, the calculated phonon dispersion curves for the RS structure at ambient and high pressures indicate that the RS phase is dynamically unstable under the pressure range of 0−85 GPa. Thus, the RS structure should be ruled out as the experimentally synthesized phase. No imaginary phonon frequencies are observed in the whole Brillouin zone (BZ), indicating that the ZB phase is dynamically stable at 0 GPa. Interestingly, it is evident that the phonon frequency of two transverse optical (TO) modes become imaginary above 7.2 GPa at the Brillouin zone boundary of the M point in the ZB structure, suggesting that it is dynamically unstable at high pressures.

As mentioned above, the platinum sublattice should be fixed in exploring crystal structures of PtC. Therefore, our structural design was studied via separate calculations of moving a carbon atom along the diagonal direction of the platinum sublattice at different pressures, and then we fully optimized all the designed structures until the energy converges. Each structure was named by the coordinate of the carbon atom along the x axis; e.g., when carbon atoms occupy (0.25, 0.25, 0.25) and (0.50, 0.50, 0.50) positions, the crystal structures are named as PtC-0.25 (ZB) and PtC-0.50 (RS), respectively. The calculated enthalpy curves under different pressures are shown in Figure 3. These results clearly show that the RS structure is not located at the enthalpy minimum at all calculated pressure points, indicating that the RS structure cannot be the experimental structure, which is consistent with our dynamical calculations. In the meanwhile, it is clearly seen that the structures corresponding to the enthalpy minima are located in PtC-0.25 (ZB) at 0 GPa, which support that the synthesized PtC is crystallized in the ZB structure at 0 GPa. Remarkably, ZB and PtC-0.47, PtC-0.20 and PtC-0.47, and PtC-0.20 and PtC-0.47 are located in the local minima on the lattice energy surface at 30, 60, and 85 GPa, respectively. Importantly, it is found that the enthalpy curve became smoothly with the rising pressure, which is rooted in the close structural relationship between these phases. The enthalpy barriers are thus very low and easy to overcome at the experimental (room) temperature. This suggests that, although there is no obvious change in the experimental X-ray diffraction, the positions of carbon atoms are fluctuating with a tiny barrier in the platinum fcc sublattices under high pressure, viz., thermal fluctuation among these structural forms. This well explains the fact that PtC may adopt a thermal fluctuation structure at high pressure. However, when it is quenchable to low pressure, it gradually becomes the ZB phase.

As one of the potential candidates for superhard materials, the mechanical properties of the ambient phase are important for the industrial applications. The elastic constants C_{ij} of the ZB phase have been calculated using the strain−stress method and are listed as the following: C_{11} = 286.5 GPa, C_{12} = 236.2 GPa, and C_{44} = 62.5 GPa, which satisfy the elastic stability criteria:[39] $C_{11} > 0$, $C_{44} > 0$, $C_{11} > |C_{12}|$, and $(C_{11} + 2C_{12}) > 0$. The calculated bulk modulus (B) of PtC reaches 253 GPa, much higher than that of pure platinum metal (230 GPa), implying that PtC is an ultra-incompressible material. The ratio between the bulk modulus and the shear modulus (G, 48 GPa) can be used to predict the brittle or ductile behavior of materials.[40] The calculated B/G for the ZB phase reaches 5.91, which is far above the criteria (1.75) for a ductile material. Poisson's ratio (ν) provides important information about the characteristics of the bonding forces; for example, it characterizes the stability of the crystal against shearing strain. Our calculations indicate that the Poisson's ratio of PtC is 0.42. With such a high Poisson's ratio, the synthesized PtC would possess large anisotropy.

The elastic anisotropy factors derived from the phonon-focusing properties of the slower mixed modes for cubic PtC are studied.[41] $C_L = C_{44} + (C_{11} + C_{12})/2$ = 323.9 GPa; $A\_100 = 2C_{44}/(C_{11} - C_{12})$ = 2.485; $A\_110 = C_{44}(C_L + 2C_{12} + C_{11})/(C_L C_{11} + C_{11}^2)$ = 0.455. It is found that the elastic anisotropy for the [100] planes is larger than that for the [110] planes. In order to describe the elastic behavior of a crystal, we have plotted a visualization of the elastic anisotropy obtained by the

dx.doi.org/10.1021/ic5006133 | Inorg. Chem. 2014, 53, 5797−5802

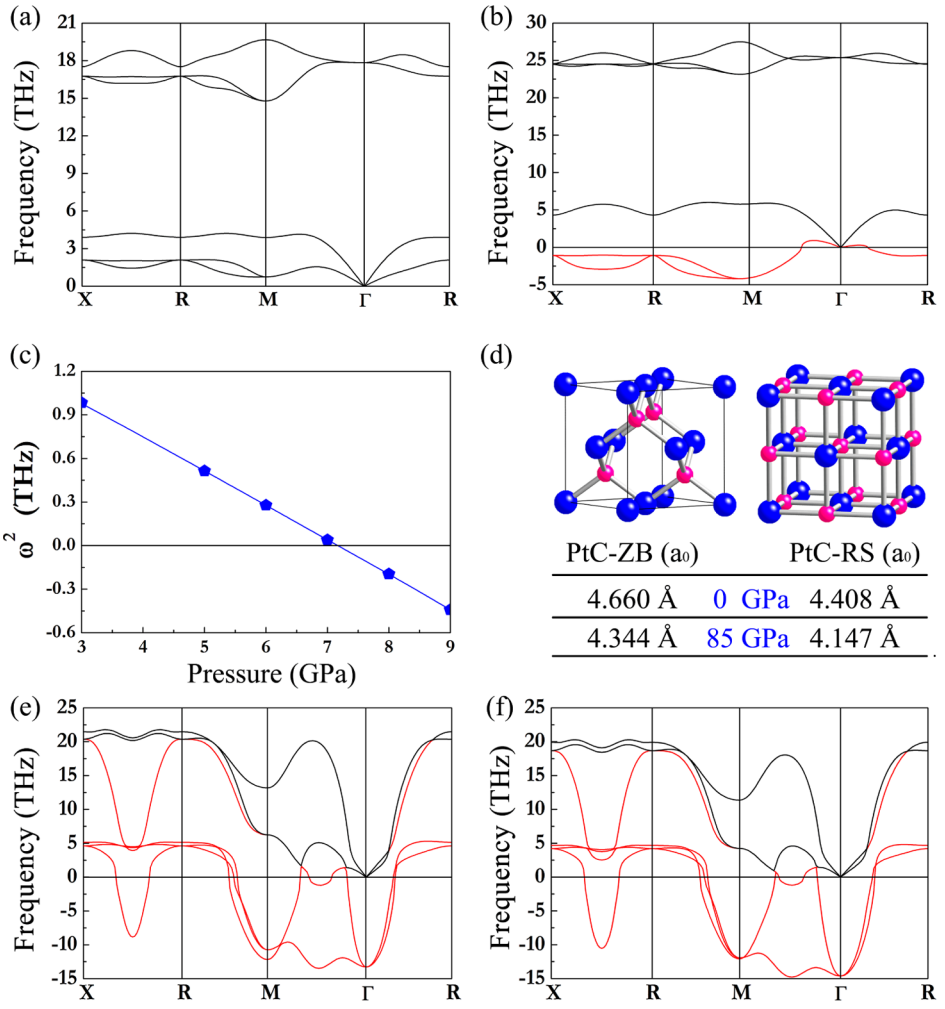

Figure 2. Calculated phonon spectra of the ZB structure at 0 (a) and 85 GPa (b). (c) The calculated phonon frequency ω^2 at the M point (0.5, 0.5, 0) in ZB as a function of pressure. The solid line through the data points is a linear fit. (d) Crystal structures and the lattice constant of the ZB and RS structures. Large and small spheres represent platinum and carbon atoms, respectively. The calculated phonon spectra of the RS structure at 0 (e) and 85 GPa (f).

dependence of Young's modulus on a direction in a crystal. For cubic materials, it is described by the following equation

$$E^{-1} = s_{11} - \beta_1(\alpha^2\beta^2 + \alpha^2\gamma^2 + \beta^2\gamma^2) \quad (1)$$

where α, β, and γ are the direction cosines of the tensile stress direction, $\beta_1 = 2s_{11} - 2s_{12} - s_{44} < 0$, and s_{11}, s_{22}, and s_{44}, are the elastic compliance constants.[42] The relationships between the elements of the matrix representation of tensor s and those of the matrix representation of tensor c in Voigt's contracted notation are $s_{11} = (C_{11} - C_{12})/(C_{11}^2 + C_{11}C_{12} - 2C_{12}^2) = 1.318 \times 10^{-4}$ GPa^{-1}, $s_{22} = C_{12}/(C_{11}^2 + C_{11}C_{12} - 2C_{12}^2) = 6.188 \times 10^{-4}$ GPa^{-1}, and $s_{44} = 1/C_{44} = 1.600 \times 10^{-2}$ GPa^{-1}. A well-pronounced isotropy and the cross sections in the yz plane for ZB phase are shown in Figure 4a,b, respectively. For a perfectly isotropic medium, the surface would be a sphere. Analytical equations for the determination of the maximum and minima values of Young's moduli are $E_{min} = 3/(s_{11} + 2s_{12} + s_{44})$ and $E_{max} = 1/s_{11}$, if $\beta_1 < 0$.[43] The "max" and "min" subscripts should be interchanged if $\beta_1 > 0$. For the cubic ZB phase, the estimated E_{max} and E_{min} values are 758.7 GPa along the [100] directions and 101.0 GPa along the [111] directions, respectively. These above analyses indicate that ZB PtC has large elastic anisotropy, which is consistent with the calculated Poisson's ratio. Previous theoretical studies suggest that the hardness of transition-metal compounds can be calculated by the hardness model[35]

$$H_v = 1051N_e^{2/3}d^{-2.5}e^{-1.191f_i - 32.2f_m^{0.55}} \quad (2)$$

where N_e is the electron density of valence electrons per Å^3, d is the bond length, and f_i is the ionicity of the chemical bond in the crystal on the Phillips scale. The theoretical f_i and f_m are 0.224 and 1.949, respectively. The simulated Vickers hardness value is 33.1 GPa for ZB PtC, lower than the criterion of superhard material (40 GPa), but higher than the standard value of hard material (20 GPa).

In order to have a better understanding of the mechanical properties, the ideal tensile and shear strength of ZB PtC are particularly important. The tensile stresses along three symmetric crystallographic directions are calculated for the purpose of identifying the weakest tensile direction. The critical shear stresses along various directions are then calculated by applying shear deformations in the easy-slip plane. The calculated tensile stress−strain relations for the ZB phase in the three principal symmetry crystallographic directions ([001], [110], and [111]) presented in Figure 5a show that PtC has the weakest responses in the [110] direction. Generally speaking, covalent solids would show sudden "hard" breaking shortly past the elastic limit;[44,45] after that, they cannot resist the tensile force in

dx.doi.org/10.1021/ic5006133 | Inorg. Chem. 2014, 53, 5797−5802

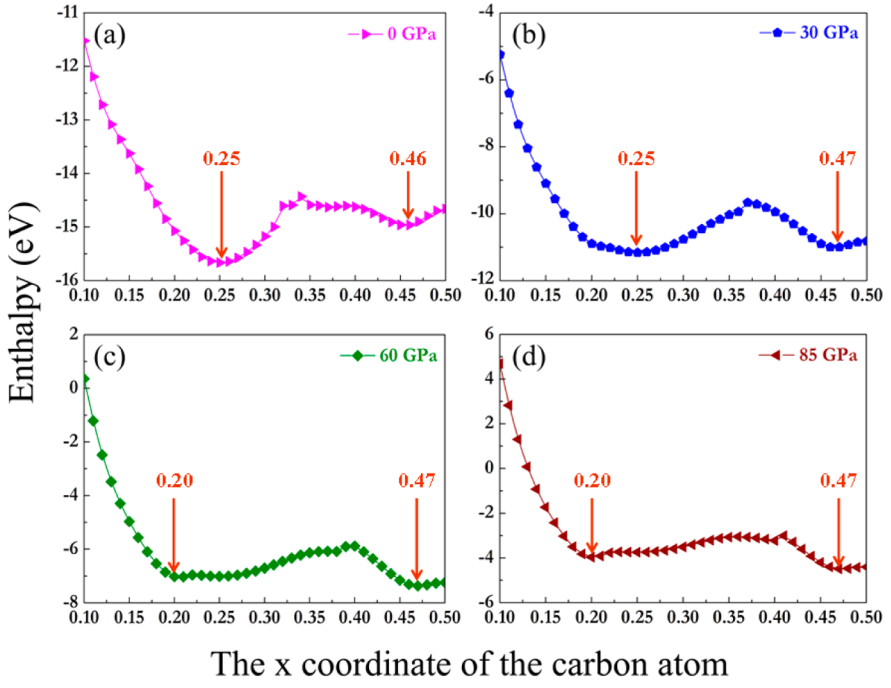

Figure 3. Calculated enthalpy curves with respect to atomic displacement at (a) 0, (b) 30, (c) 60, and (d) 85 GPa, respectively.

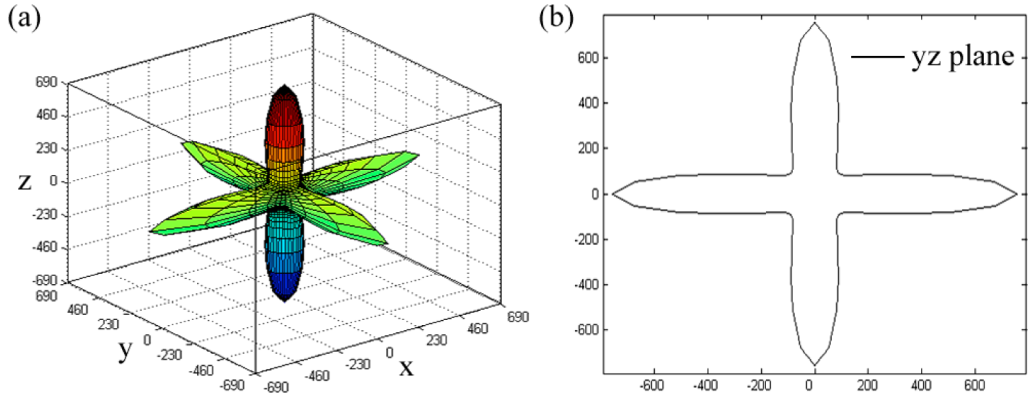

Figure 4. (a) Directional dependence of Young's modulus for PtC. (b) The projection in the *yz* plane.

Table 1. Variations of Calculated Pt−C Bond Lengths and Bond Angles with Strain under Uniaxial [110] Loading from T_0 to T_3 and the Variations of Pt−C Bond Lengths and Bond Angles with Strain in Easy-Slip Planes (110) under Uniaxial [1$\bar{1}$0] Loading from T_0 to T_4[a]

		bond length (Å)			bond angle (deg)		
		Pt1−C	Pt2−C	Pt3−C	α	β	γ
tensile	T_0	2.018	2.018	2.018	109.5	109.5	109.5
	T_1	2.068	2.067	2.002	106.2	107.9	106.8
	T_2	2.066	2.062	2.006	91.6	101.6	120.6
	T_3	2.248	2.246	2.027	84.5	96.2	114.7
		Pt1−C1	Pt2−C2	Pt3−C3	α	β	
shear	T_0	2.018	2.018	2.018	109.5	109.5	
	T_1	2.058	2.066	2.055	97.3	95.4	
	T_2	2.098	2.049	2.050	87.0	87.0	
	T_3	2.241	2.083	2.083	80.3	82.8	
	T_4		2.174	2.174		80.4	

[a]The angles α, β, and γ refer to Pt1−C−Pt3, Pt3−C−Pt4, and Pt2−C−Pt3 in tensile and the angles α and β refer to Pt1−C1−Pt4 and Pt3−C3−Pt5 in shear, respectively.

the later stretching process, which leads to the calculated instantaneous resist tensile capacity fall to zero. As shown in Figure 5, a novel fluctuating behavior occurs in the current calculation. Interestingly, PtC achieves a second tensile strength peak of 37.0 GPa, which is nearly 4 times greater than the first one (10.7 GPa). To understand this intriguing phenomenon,

dx.doi.org/10.1021/ic5006133 | Inorg. Chem. 2014, 53, 5797−5802

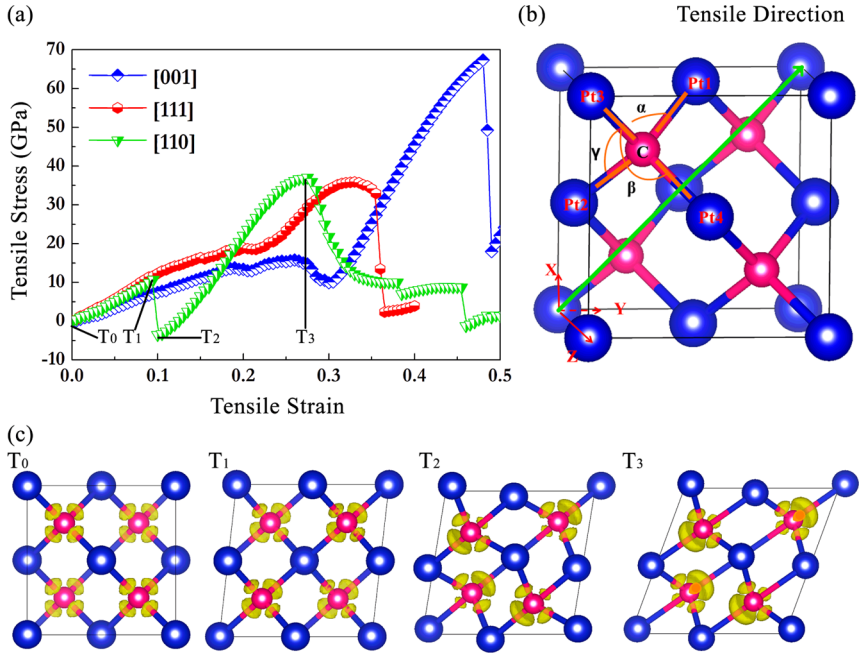

Figure 5. (a) The calculated tensile stress versus tensile strain for PtC in the three principal symmetry crystallographic directions. (b) The weakest tensile direction [110] in polyhedral PtC. (c) The ELF of T_0, T_1, T_2, and T_3 structures under strain.

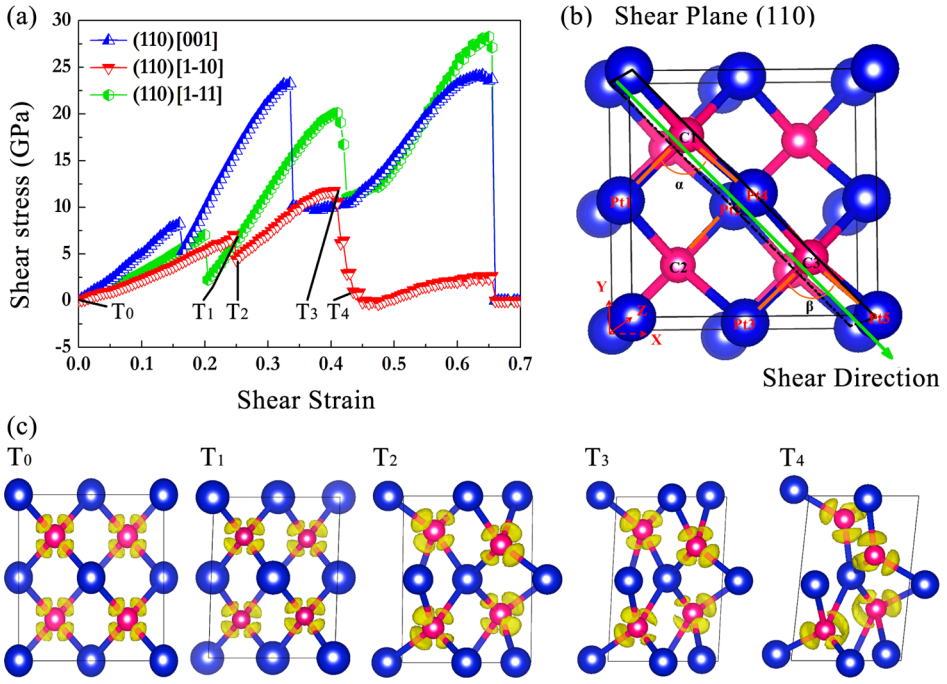

Figure 6. (a) The calculated shear stress versus shear strain for PtC in the three principal symmetry crystallographic directions. (b) The slip direction $(110)[1\bar{1}0]$ in polyhedral PtC. (c) The ELF of T_0, T_1, T_2, T_3, and T_4 structures under strain.

the analyses of the electron localization function (ELF),[46,47] bond lengths, and bond angles have been well-presented. The four Pt atoms which are the first nearest neighbors of a C atom are labeled Pt1 to Pt4. We focus our analyses on the changes of the bond lengths and bond angles among five selected atoms Pt1, Pt2, Pt3, Pt4 and C. They are responsible for the large plastic deformation in the unit cell as indicated in Figure 5. The angle Pt1−C−Pt3 (α) is equal to the angle Pt1−C−Pt4, and the angle Pt2−C−Pt3 (β) sis equal to the angle Pt2−C−Pt4 due to the crystal symmetry. The evolution of the covalent bond lengths and bond angles with strain under uniaxial [110] loading from T_0 to T_3 are listed in Table 1. It is found that the first steep drop is caused by the change of bond angle α. From T0 to T1, the marked bonds (Pt3−C and Pt4−C) become much longer, and α is gradually close to 90° (corresponding to the process T_1 to T_2). Then, both bonds have no contribution to resist the tensile strength, resulting in a sudden release in tensile capacity. In the later stretching process, α is smaller and smaller, leading to the projection in the [110] direction and higher stretching force.

dx.doi.org/10.1021/ic5006133 | Inorg. Chem. 2014, 53, 5797−5802

The further calculated shear stress−strain relations of PtC are shown in Figure 6a. The strain−stress relationship also exhibits a fluctuating behavior associated with the change of bonds. The results identify the first and second peak stress of 7.0 and 11.8 GPa in the $[1\bar{1}0]$ direction in the easy-slip plane (110), respectively. The calculated bond lengths and bond angles with strain under uniaxial $[1\bar{1}0]$ loading from T_0 to T_4 are listed in Table 1. In the process from T_0 to T_1, the bond angles α and β gradually close to 90°. Then, the two bonds (Pt1−C1 and Pt3−C3) are perpendicular to the shear direction (α and β are approximately equal to 90°); the bonds have no effect to resist the shear force, leading to the first drop in the shear stress−strain relation. After that, α and β become smaller and smaller, resulting in PtC having a stronger ability to resist the shear force. Under a large strain of 0.405, the breaking of bond Pt1−C1 leads to the collapse of the structure (from T_3 to T_4). The current results proposed an intriguing mechanism for the changes of bond angles in the process of stretching, which could expand our knowledge on the strength of heavy transition-metal carbides.

CONCLUSIONS

Here, the crystal structure and mechanical properties of PtC were investigated using first-principles calculations. The synthesized PtC has a zinc blende structure at ambient conditions, while the position of carbon atoms in PtC are not fixed and fluctuating in the platinum sublattice at high-pressure conditions (above 7.2 GPa). The theoretical Poisson's ratio and elastic anisotropic factors suggest that the synthesized PtC is highly anisotropic and strongly dependent on the crystallographic direction. The fluctuating strain−stress relationship is attributed to the evolution of bond angles in the process of stretching. These results significantly improve our understanding of the structural identification and mechanical properties of PtC and will stimulate further theoretical and experimental studies for heavy transition-metal carbides.

AUTHOR INFORMATION

Corresponding Authors

*Phone: +86-431-85167557. E-mail: liquan777@jlu.edu.cn (Q.L.).

*Phone: +86-431-85167557. E-mail: huiwang@calypso.cn (H.W.).

Notes

The authors declare no competing financial interest.

ACKNOWLEDGMENTS

This work is supported by the China 973 Program (2011CB808200), the Natural Science Foundation of China under 11274136, 11025418, 51202084, 11104104, and 91022029, the 2012 Changjiang Scholars Program of China, and the Changjiang Scholar and Innovative Research Team in University (IRT1132). Parts of the calculations were performed in the High Performance Computing Center (HPCC) of Jilin University.

REFERENCES

(1) Li, Q.; Wang, H.; Ma, Y. *J. Superhard Mater.* **2010**, *32*, 192−204.
(2) Tian, Y.; Xu, B.; Zhao, Z. *Int. J. Refract. Met. Hard Mater.* **2012**, *33*, 93−106.
(3) Zhang, X.; Wang, Y.; Lv, J.; Zhu, C.; Li, Q.; Zhang, M.; Li, Q.; Ma, Y. *J. Chem. Phys.* **2013**, *138*, 114101.
(4) Li, Q.; Wang, M.; Oganov, A. R.; Cui, T.; Ma, Y.; Zou, G. *J. Appl. Phys.* **2009**, *105*, 053514.
(5) Pan, Z.; Sun, H.; Chen, C. *Phys. Rev. B* **2004**, *70*, 174115.
(6) Rignanese, G.-M.; Charlier, J.-C.; Gonze, X. *Phys. Rev. B* **2002**, *66*, 205416.
(7) Li, Q.; Liu, H.; Zhou, D.; Zheng, W.; Wu, Z.; Ma, Y. *Phys. Chem. Chem. Phys.* **2012**, *14*, 13081−13087.
(8) Lyakhov, A. O.; Oganov, A. R.; Valle, M. *Comput. Phys. Commun.* **2010**, *181*, 1623−1632.
(9) Kaner, R. B.; Gilman, J. J.; Tolbert, S. H. *Science* **2005**, *308*, 1268−1269.
(10) Li, Y.; Li, Q.; Ma, Y. *Europhys. Lett.* **2011**, *95*, 66006.
(11) Cumberland, R. W.; Weinberger, M. B.; Gilman, J. J.; Clark, S. M.; Tolbert, S. H.; Kaner, R. B. *J. Am. Chem. Soc.* **2005**, *127*, 7264−7265.
(12) Young, A. F.; Sanloup, C.; Gregoryanz, E.; Scandolo, S.; Hemley, R. J.; Mao, H.-k. *Phys. Rev. Lett.* **2006**, *96*, 155501.
(13) Li, Y.; Wang, H.; Li, Q.; Ma, Y.; Cui, T.; Zou, G. *Inorg. Chem.* **2009**, *48*, 9904−9909.
(14) Zhang, M.; Yan, H.; Wei, Q.; Wang, H. *Europhys. Lett.* **2012**, *100*, 46001.
(15) Li, Q.; Zhou, D.; Zheng, W.; Ma, Y.; Chen, C. *Phys. Rev. Lett.* **2013**, *110*, 136403.
(16) Ono, S.; Kikegawa, T.; Ohishi, Y. *Solid State Commun.* **2005**, *133*, 55−59.
(17) Sun, X.; Zeng, Z.; Song, T.; Fu, Z.; Kong, B.; Chen, Q. *Chem. Phys. Lett.* **2010**, *496*, 64−67.
(18) Sun, X.; Chu, Y.; Quan, W.; Chen, Q.; Chen, X.; Song, T.; Tian, J. *J. Mater. Sci.* **2013**, *48*, 1660−1668.
(19) Sun, X.-W.; Chen, Q.-F.; Cai, L.-C.; Chen, X.-R.; Jing, F.-Q. *Chem. Phys. Lett.* **2011**, *516*, 158−161.
(20) Rabah, M.; Rached, D.; Ameri, M.; Khenata, R.; Zenati, A.; Moulay, N. *J. Phys. Chem. Solids* **2008**, *69*, 2907−2910.
(21) Ivanovskii, A. L. *Russ. Chem. Rev.* **2009**, *78*, 303−318.
(22) Li, L.; Yu, W.; Jin, C. *J. Phys.: Condens. Matter* **2005**, *17*, 5965.
(23) Sun, X. W.; Chen, Q. F.; Chen, X. R.; Cai, L. C.; Jing, F. Q. *J. Appl. Phys.* **2011**, *110*, 103507.
(24) Peng, F.; Fu, H. Z.; Yang, X. D. *Solid State Commun.* **2008**, *145*, 91−94.
(25) Zaoui, A.; Ferhat, M. *Solid State Commun.* **2011**, *151*, 867−869.
(26) Fan, C.; Sun, L.; Wang, Y.; Liu, R.; Zeng, S.; Wang, W. *Phys. B: Condens. Matter* **2006**, *381*, 174−178.
(27) Deligoz, E.; Ciftci, Y.; Jochym, P.; Colakoglu, K. *Mater. Chem. Phys.* **2008**, *111*, 29−33.
(28) Fan, C.-Z.; Zeng, S.-Y.; Zhan, Z.-J.; Liu, R.-P.; Wang, W.-K.; Zhang, P.; Yao, Y.-G. *Appl. Phys. Lett.* **2006**, *89*, 071913.
(29) Ceperley, D. M.; Alder, B. *Phys. Rev. Lett.* **1980**, *45*, 566.
(30) Ihm, J.; Zunger, A.; Cohen, M. L. *J. Phys. C: Solid State Phys.* **1979**, *12*, 4409.
(31) Kresse, G.; Furthmüller, J. *Phys. Rev. B* **1996**, *54*, 11169−11186.
(32) Blöchl, P. E. *Phys. Rev. B* **1994**, *50*, 17953−17979.
(33) Monkhorst, H. J.; Pack, J. D. *Phys. Rev. B* **1976**, *13*, 5188−5192.
(34) Hill, R. *Proc. Phys. Soc.* **1952**, *65*, 349.
(35) Guo, X.; Li, L.; Liu, Z.; Yu, D.; He, J.; Liu, R.; Xu, B.; Tian, Y.; Wang, H.-T. *J. Appl. Phys.* **2008**, *104*, 023503.
(36) Roundy, D.; Krenn, C.; Cohen, M. L.; Morris, J., Jr. *Philos. Mag. A* **2001**, *81*, 1725−1747.
(37) Roundy, D.; Krenn, C. R.; Cohen, M. L.; Morris, J. W., Jr. *Phys. Rev. Lett.* **1999**, *82*, 2713−2716.
(38) Zhang, Y.; Sun, H.; Chen, C. *Phys. Rev. Lett.* **2004**, *93*, 195504.
(39) Born, M.; Misra, R. D. *On the Stability of Crystal Lattices*; Cambridge University Press: London, 1940.
(40) Pugh, S. *Philos. Mag.* **1954**, *45*, 823.
(41) Lau, K.; McCurdy, A. K. *Phys. Rev. B* **1998**, *58*, 8980.
(42) Nye, J. F. *Physical Properties of Crystals*; Oxford University Press: London, 1985.
(43) Cazzani, A.; Rovati, M. *Int. J. Solids Struct.* **2003**, *40*, 1713−1744.
(44) Zhang, Y.; Sun, H.; Chen, C. *Phys. Rev. Lett.* **2004**, *93*, 195504.
(45) Zhang, Y.; Sun, H.; Chen, C. *Phys. Rev. Lett.* **2005**, *94*, 145505.
(46) Becke, A. D.; Edgecombe, K. E. *J. Chem. Phys.* **1990**, *92*, 5397.
(47) Silvi, B.; Savin, A. *Nature* **1994**, *371*, 683−686.